Proceedings of the 5th IBPC, Kyoto, Japan, May 28-31, 2012

Experimental investigation of the impact of room/system design on mixed convection heat transfer

Kim Goethals [1], Marc Delghust [1,2], Gilles Flamant [3], Michel De Paepe [4] Arnold Janssens [1]

[1] *Research Group of Building Physics, Construction and Services, Ghent University, Ghent, Belgium*
[2] *PhD-fellowship of the Research Foundation Flanders (FWO)& the Flemish Institute for Technological Research (VITO)*
[3] *Laboratory Energy Characteristics, Belgian Building Research Institute, Limelette, Belgium*
[4] *Research Group of Applied Thermodynamics and Heat Transfer, Ghent University, Ghent, Belgium*

Keywords: night cooling, experiment, design, convective heat transfer

ABSTRACT

Multizone building energy simulation programs become popular among building designers. They include a wide variety of techniques and advanced heat transfer models, yet require only limited computation time. Unfortunately, the use of correlations to predict the convective heat transfer undermines their reliability. The correlations actually apply only to specific cases. Meanwhile, convective heat transfer modelling is particularly important in mixed convection regimes with high ventilation rates. It is self-evident that researchers would investigate to what extent including more room/system design parameters is necessary to model mixed convection heat transfer. The authors of this study imitated sequences of typical mixed convection cooling regimes (a day regime possibly preceded by night cooling) in a modified PASLINK cell and varied the air supply/exhaust configuration and added to some cases a thermally massive floor. The analysis was based on airflow data and the convective heat flux. The results indicate that the air supply/exhaust configuration is important when high ventilation rates are combined with heterogeneously distributed thermal mass. Existing convection correlations cannot predict the convective heat flux accurately for the studied cases.

1. Introduction

To analyse the complex behaviour of building energy use, building designers often use stand-alone multizone Building Energy Simulation (BES) programs. Such tools include a variety of techniques and advanced heat transfer models, yet require only limited computation time. One of the reasons for this fast execution speed is the way the interior convective heat transfer is modelled. Most BES programs employ the so-called well-mixed assumption. This treats the room air as uniform and characterizes the surface convective heat flux q_{conv} by the product of a convective heat transfer coefficient h_{conv} and the temperature difference between the room air and the internal surface (T_w-T_a). Such convection coefficients usually rely on correlations derived from experimental data. The researchers in question copied in a simplified experimental design the boundary conditions applicable to a specific mechanism of fluid flow, flow regime and geometry and related the derived convective heat transfer coefficient with some term expressing either a temperature difference or a velocity, depending on the studied mechanism of fluid flow (natural or forced convection). Mixed convection correlations were obtained by blending natural and forced convection correlations. Some researchers even included a characteristic dimension to be able to asses scale effects (Goethals et al., 2011). However, there is one important shortcoming of this approach: the convection correlations apply merely to specific cases. The researchers only included a limited number of room/system design parameters. For example, they are only valid for one diffuser type at a particular location. Meanwhile, several studies indicated the importance of accurately modelling the interior convective heat transfer. For example, the coordinated Annex 21 project (Lomas et al., 1994) acknowledged the dominant role of convective heat transfer in the building's energy balance. Certainly in mixed convection cases with high ventilation rates, such as night cooling, convective heat transfer modelling is important (Goethals et al., 2011). So it is self-evident that researchers would investigate to what extent including more room/system design parameters is necessary to model (mixed) convective heat transfer. Previous works (e.g. (Artmann et al., 2010)) have already given the initial impetus. Underlying study continues to work on this. The authors imitated sequences of typical mixed convection cooling regimes (a typical day regime possibly followed by night cooling) in and adapted PASLINK cell. Here, they varied the air supply/exhaust configuration and added to some cases a floor with a high heat storage capacity.

2. Experiment design

2.1 Test room setup

A PASLINK cell at the Belgian Building Research Institute (BBRI) in Limelette (Belgium) accommodated the experiments. The development of this type of highly standardized test cell started with the PASSYS project. The researchers involved attempted to increase confidence in energy conscious and passive solar building products and evaluation techniques. To this end, they built test cells that enabled to define the thermal performance of building components exposed to real climate conditions. Such a test cell was constructed as a prefabricated, well-insulated structure comprising a test room and a service room. The test room allowed for measurements of heat transfer through all enclosure surfaces. Later on, part of the COMPASS project, so-called pseudo-adiabatic shell (PAS) panels were added to the inside of some PASSYS test cells to improve the test cell performance and measurement accuracy. These calorimetric layers consisted of an electric heating foil and a sequence of insulating and conductive materials (Figure 1). The current name of the cells refers to the last large-scale application, i.e. the PASLNK project. This study did not make changes to the test facilities as it focussed on the dynamic analysis and test methodology for building component evaluation under real outdoor conditions. In conclusion, the advantages of this type of test cell lied in the well-controlled, real room sized environment and the absence of occupancy effects. Besides,

the presence of the PAS panels enabled to determine more accurately the conductive heat flux and, thus, the convective heat flux. As a consequence, the test cell was found adequate to investigate convective heat transfer.

Yet, the cell needed modifications, as shown in Figure 2. First, the measurement bay which was originally used for adding building components, was filled with a copy of the current side walls. Further, a separation wall made of 0.20m expanded polystyrene (EPS) was installed in the test room to isolate the air handling unit (AHU) in a second service room. This created a new geometrically simple test room, having internal dimensions of 3.75m in length, 2.51m in width and 2.50m in height. In the upper part of this new separation wall, at 0.20m from the ceiling, two openings were foreseen: one in the symmetry plane and one at 0.20m from the east side wall. At the lower part, one opening was located in the symmetry plane at 0.20m above the floor (Figure 3). Each opening could be used to exhaust (directly linked with the second service room) or supply (grille diffuser connected with the AHU) air to the test room or could simply be closed. Next, a heat source, which could be activated, was located between zone 1 and zone 2 (grey rectangular in Figure 2 and Figure 3). The design of this heat source was partly based on DIN 4715 (DIN, 1993). It was a closed aluminium box having dimensions of 0.40m in length, 0.25m in width and 1.00m in height, supported by 0.10m high legs. Its outside was finished with a paint similar to the one of the enclosure surfaces. At the inside, three electrical bulbs could produce a heat load of 77.2W while two fans (2 x 1.4W) guaranteed a uniform temperature distribution. Finally, some experimental runs included a double layer of concrete tiles on the floor.

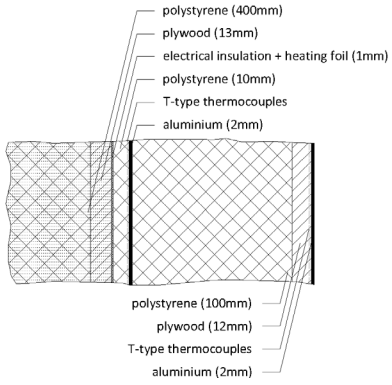

Figure 1 PAS (black) and part of the original envelope (grey)

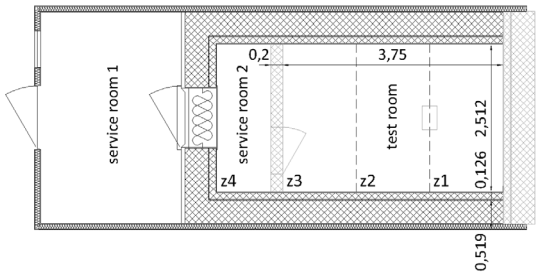

Figure 2 Plan of the PASLINK cell (black) with modifications (grey) (dimensions in meters)

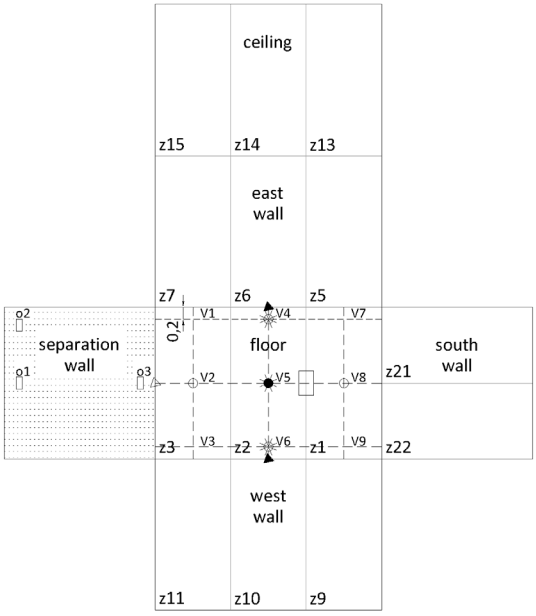

Figure 3 PAS panel distribution and measurement locations: a) intersection striped lines: air temperature at 0.20m, 1.25m and 2.3m height, b) ✳: air temperature at 0.02m, 0.04m, 0.10m, 0.20m, 1.25m, 2.30m, 2.40m, 2.46m and 2.48m height, c) ○ : velocity measurement at 1.25m height, d) ● : air velocity at 00.20m, 1.25m and 2.30m height, e) △: surface temperature at 0.20m, 1.25m and 2.30m height, f) ▲ : surface temperature at 0.20m, 1.25m and 2.30m height, g) heat flux sensors on the floor near v2, v5 and v8

2.2 Test equipment

As mentioned before, the PAS panels acted as large heat flux sensors. The electric heating foil in each panel was located in between the original outside envelope and a 0.10m EPS layer. The aluminium layers on either side of this 0.10m EPS layer created isothermal planes and each one of them was equipped with a set of eight T-type thermocouples (accuracy ±0.19K) connected in series. In the experiments of this study, the operation of each heating foil depended only on the temperature set at the outer aluminium plate. This left opportunity to derive the conductive heat flux through the PAS and, thus, the convective heat flux at the interior surface – similar to preceding studies. To check the heat flux through the concrete tiles three heat flux sensors were fixed to the interior surface of the tiles, near locations v2, v5 and v8 (Figure 3). The interior of the test room was also equipped with additional T-type thermocouples. First of all, at the same locations of the three heat flux sensors, thermocouples were installed on top and in between the two layers of concrete tiles. Further, thermocouples fixed to the interior side of PAS panels z6 and z10 measured the local surface temperature at 0.20m, 1.25m and 2.30m height. These enabled to check whether the highly conductive aluminium sheets guaranteed a uniform temperature distribution. Further, thermocouples fixed to the centre of the EPS separation wall and of the respective five surfaces of the heat source measured the surface temperature. Also in the air supply and exhaust thermocouples were installed. Furthermore, more thermocouples, fixed to nine vertical ropes measured every minute the temperature distribution in the room. In general, the air temperature was monitored at three heights (0.20m, 1.25m and 2.30m). However, at positions v4, v5 and v6, additional sensors at smaller distances (0.02, 0.04m and 0.10m) from the horizontal

surfaces recorded the local air distribution. To perturb the airflow as little as possible, the original radiation shields around the thermocouples were removed. In this experimental setup, radiation introduced an error in measurement which was smaller than the thermocouple accuracy (±0.19°C). Figure 4 illustrates this by setting the thermocouple reading T_{TC} against the calculated air temperature $T_{a,l}$. $T_{a,l}$ was derived from the steady-state heat balance of the thermocouple (Eq. (1)).

$$T_{TC} = \frac{h_{conv} \cdot T_{a,l} + h_{rad} \cdot T_{w,avg}}{\left(h_{conv} + h_{rad}\right)} \quad (1)$$

This equation states that the thermocouple reading T_{TC} is the weighted average of the air temperature $T_{a,l}$ and the mean surface temperature $T_{w,avg}$ of the surroundings, defined by the convective heat transfer coefficient h_c and the radiative heat transfer coefficient h_r. NBN (2009) in conjunction with view factor calculation helps to derive h_r. Determination of h_c relies on work of Wang and Travnicek (2001) on convective heat transfer for crossflow over a circular cylinder. Further, omnidirectional thermal anemometers measured every minute the air velocity at seven points (Figure 3). The measurement accuracy was limited to 3.0% of the recording and an additional 1.0% of the selected measurement range (0.05m/s to 2.5m/s).

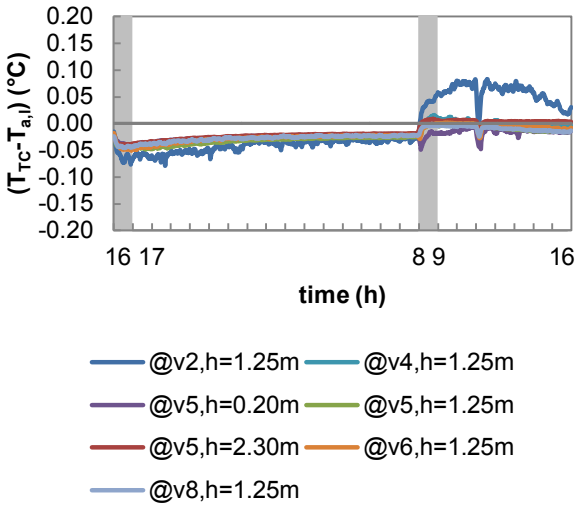

Figure 4 Comparison of thermocouple reading and air temperature during the last 24h of run 3 (N;c;T) (for references to colour check digital version)

2.3 Test procedure

During the experiments, the following parameters were varied: the volumetric flow rate n·V, the air supply temperature T_{sup}, the temperature measured at the outer aluminium layer in the PAS panels $T_{alu,outer}$, the operation of the heat source, the presence of concrete tiles on the floor and the locations of the air supply/exhaust. The experiments imitated a 24h cycle which comprised two distinct convection regimes as shown in Figure 5. From 8h until 16h the boundary conditions led to a typical mixed convection regime. The AHU supplied 36m^3.h^{-1} of air at 23.5°C and the heat source of 80.0W was active. During the following period, i.e. from 16h until 8h, everything but the heating by foils could be shut down or night cooling could be imitated (n·V=188m^3.h^{-1} and T_{sup}=16.5°C, inactive heat source). These two possible sequences were combined with two different amounts of thermal mass (with and without concrete tiles on the floor) and two air supply/exhaust configurations (o1/o3 and o3/o1), which resulted in a total of eight experimental runs as shown in Table 1. Each run lasted about six days. Note in this table the codes of the respective runs: the capital letters N, C and T indicate that night cooling was applied, concrete tiles were present respectively the air supply was located at the top. Regular letters represent the other possibilities. Further note that the results of the period of time in which the AHU and the heat source were switched off, are usually omitted in the analyses to come.

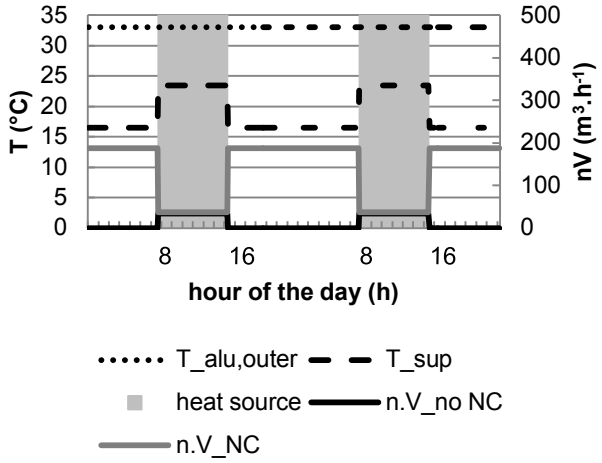

Figure 5 Boundary conditions for the experiments

Table 1 Overview of the experiments (for references to colour, check digital version)

	night cooling?	concrete tiles?	supply at top?
Run 1 (N;C;T)	•	•	•
Run 2 (N;C;t)	•	•	
Run 3 (N;c;T)	•		•
Run 4 (N;c;t)	•		
Run 5 (n;C;T)		•	•
Run 6 (n;C;t)		•	
Run 7 (n;c;T)			•
Run 8 (n;c;t)			

3. Analysis method

3.1 Radiation/conduction model

This study calculates the convective heat flux from temperature measurements, like many previous studies. However, the derivation approach differs in one or more aspects. First, this study does not aim at steady-state boundary conditions. It actually investigates the transient response of a room induced by step changes. As a consequence, a transient thermal analysis is necessary to derive the time-varying heat flux. Secondly, no surface inside the adapted PASLINK cell has a reflective finish and, thus, it is primordial to take radiation into account. For these reasons, this study deploys a conduction/radiation model which solves a heat balance at a given PAS panel (Eq. (2)). The reason why this in-house conduction/radiation model is used, is because it runs faster in comparison with commercial alternatives. With this, this study follows the approach suggested by Artmann et al. (2010).

$$q_{conv}(t) = q_{cond}(t) - q_{rad}(t) \quad (2)$$

A 1-D finite volume model, with Crank-Nicholson time stepping, calculates the transient conductive heat flux through a PAS panel. On the assumption of uniform conductivity and uniform grid spacing, the used discretised heat conduction equation comes down to Eq. (3). This equation is used to predict the temperature at point i at time m.

$$\rho \cdot c \frac{\Delta x}{\Delta t} \cdot \left(T_i^m - T_i^{m-1}\right) = 0.5 \cdot \left[\frac{\lambda\left(T_{i-1}^m - T_i^m\right)}{\Delta x} - \frac{\lambda\left(T_i^m - T_{i+1}^m\right)}{\Delta x} \right] + 0.5 \cdot \left[\frac{\lambda\left(T_{i-1}^{m-1} - T_i^{m-1}\right)}{\Delta x} - \frac{\lambda\left(T_i^{m-1} - T_{i+1}^{m-1}\right)}{\Delta x} \right] \quad (3)$$

The analysis comprises three PAS layers and a virtual layer. The three PAS layers correspond to the material layers in between the outer and inner thermocouples. Table 2 lists their respective thickness d, thermal conductivity λ and volumetric heat capacity ρc. The 0.0001m thick virtual layer, placed next to the plywood, has a negligible thermal resistance (1.10^{-8}m.K.W^{-1}) and a small volumetric heat capacity (0.01kJ.m^{-3}.K^{-1}). It actually enables to extract correctly the conductive heat flux to the inner aluminium sheet. At each time step, the conduction model applies Fourier's law of conduction to the two computing nodes in the virtual layer closest to the interior of the PASLINK cell (Eq. (4)):

$$q_{cond} = \frac{\lambda\left(T_{i-1} - T_i\right)}{\Delta x} \quad (4)$$

Table 2 Mean properties and uncertainties (95%) of the PAS layers in between the inner and outer thermocouples

Layer	d (m)	λ (W.m^{-2}.K^{-1})	ρc (kJ.m^{-3}.K^{-1})
Outer aluminium	0.002 ±10%	230 ±2%	2430 ±5%
EPS	0.100 ±0.002	0.033 ±0.002	26 ±10%
Plywood	0.012 ±5%	0.108 ±0.014	1400 ±5%

This conduction model is complemented with the ability to calculate radiant heat transfer, in conjunction with view factor calculation, for the twenty surfaces considered (i.e. fourteen PAS panels, one EPS separation wall and five surfaces of the heat source). This model assumes diffuse-grey surfaces with a non-participating medium in between (air). At each time step, it solves Eq. (5) for the unknown radiosity J_i of each surface in the room (i.e. the total radiation that leaves the surface per unit time and per unit area). The net radiant flux $q_{rad,i}$ lost by surface i then comes from Eq. (6), i.e. the difference between the radiosity J_i and the irradiation G_i (i.e. total radiation incident on the surface per unit time and per unit area).

$$J_i = \varepsilon_i \cdot \sigma \cdot T_i^4 + \left(1 - \varepsilon_i\right) \sum_{j=1}^{n} F_{ij} J_j \quad (5)$$

$$q_{rad,i} = J_i - G_i = J_i - \sum_{j=1}^{n} F_{ij} J_j \quad (6)$$

The parameter σ represents the Stefan-Boltzmann constant and F_{ij} is the view factor from surface i to surface j. Further, ε_i stands for the emissivity of each one of the surfaces i. Almost all surfaces have an emissivity of 0.88. Only the concrete tiles have a higher emissivity of 0.95. Finally, T_i equals the temperature of each one of the surfaces i. In case of a PAS panel, this corresponds to the average of the thermocouple readings at the inner part. On the other hand, in case of the EPS separation wall and the surfaces of the heat sources, the temperature T_i comes from one thermocouple reading. This conduction/radiation model was verified against the commercial software VOLTRA, confirming its precision.

The simulations use a grid size of 0.005 for the EPS layer, of 0.0005m for the plywood layer and the aluminium layer and of 0.00002m for the virtual layer. The time step size is equal to the measuring interval, i.e. 60s. A preliminary space/grid convergence study showed that these discretisation resolutions ae fine enough. Simulation results based on an eight times smaller grid or a twelve times smaller time step size differed by at most 0.005W.m^{-2} from the ones on the original resolutions. Each simulation covers 3.5 days singled out of the respective experimental campaigns. The first 2.5 days account for the unknown initial temperature distribution in the PAS; the remaining period of 1 day is used for analysis. By way of example, Figure 6 shows the calculated instantaneous convective heat flux q_{inst} at PAS panel z13 during the last 24h of run 3 (N;c;T). The graph not only depicts the predicted convective heat flux, but also the air supply temperature T_{sup}, the local air temperature $T_{a,l}$ on v8 at 2.3m height and the surface temperature T_w of PAS panel z13. The two distinct operating conditions catch the eye: the day regime and the night regime with night cooling. Next to this, each regime comprises two behaviours: a stepwise change leads to an initial steep transition of the convective heat flux followed by a quasi-exponential increase/decrease to the steady-state level (quasi-exponential because of the changing heat transfer and the time constant of the indoor air). The steep changes originate from the delayed change of the air supply temperature and the time constant of the indoor air. Therefore, further analyses of the experiments exclude the first hour of each regime (indicated by the grey zones). This also enables to calculate low-order polynomial regressions of the convective heat flux q_{regr}, on which the bulk of the following analyses build.

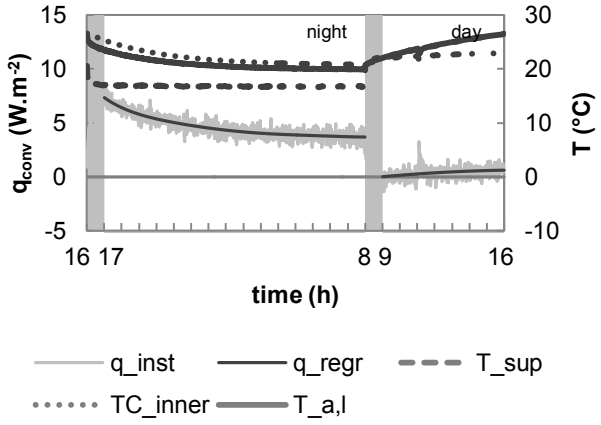

Figure 6 Comparison of thermocouple reading and air temperature during the last 24h of run 3 (N;c;T)

3.2 Uncertainty analysis

Regardless of whether model inputs are measured experimentally or obtained from literature, they cannot be assumed to be free of error. To determine how these input uncertainties impact upon the simulated heat fluxes by conduction, radiation and convection, underlying study relies on Monte Carlo Analysis. This method incorporates the influence of the whole range of variation and distribution of the input parameters and evaluates the effect of one parameter while all other parameters are varied as well. This way, the uncertainty analysis provides the range and probability density for specific confidence intervals (typically 95%). The analysis takes into account the uncertainties in the following input variables: the thickness, the thermal conductivity and the volumetric heat capacity of the considered PAS layers, the

emissivity of the inner surfaces and the thermocouple readings at the inner and outer part of the considered layers. The actual procedure starts with selecting a distribution and range for each input parameter. Aforementioned input variables are assumed to be normally distributed, having a confidence interval of 95%. Table 2 shows the mean value and associated uncertainty of the properties of the considered PAS layers. The thermal conductivities are measured on material samples from the PAS. The associated uncertainties are based on the empirical correlations of Dominguez-Munoz et al. (2010). The other parameter values and uncertainty bounds rely on produce specifications and fabrication standards (e.g. CEN (2008), ISO (2007)). The emissivity of the inner surfaces of the PAS is set to 0.88±0.05 while 0.95±0.05 applies to the concrete tiles. Finally, the uncertainty of the thermocouple reading at the inner/outer part of each PAS panel equals ±0.07°C, which is smaller than the before-mentioned uncertainty for one thermocouple, i.e. ±0.19°C. As a matter of fact, the stored temperature equals the arithmetic mean of eight thermocouple recordings, of which each covers an identical area. As highly conductive aluminium sheets assumedly guarantee a uniform temperature distribution, each thermocouple measures the same temperature. So, according to theory of error propagation, the error of eight thermocouple recordings reduces by a factor 2.8: $[8\cdot(0.19)^2]^{0.5}/8$. The uncertainty analysis continues by generating a sample from these distributions. For simplicity, this study relies on random sampling. However, to control the likely size of the sampling error, it takes a large enough sample. Then, the conduction/radiation code calculates the impact for each element of this sample, before finally deriving the uncertainty bounds. How to determine these uncertainty bounds is explained in the following. Starting with the measured temperatures at time steps T_1, T_2, …, T_m (where m=5250), simulations including different combinations of setup uncertainties E_1, E_2, …, E_n (where n=300) enables to determine the standard deviation of the resulting indeed regressed 300 fluxes for each time step $\sigma(q_{1,regr\ j})$, $\sigma(q_{2,regr\ j})$, $\sigma(\ldots)$,$\sigma(q_{m,regr\ j})$. Obviously, multiplied by ±1.96, this standard deviation defines the 95% confidence interval. Mind that this uncertainty also includes the (small) error introduced by the regression of the actual heat fluxes $q_{1,j}$, $q_{2,j}$, …, $q_{m,j}$. Figure 7 shows, by way of example, boxplots of the uncertainties of the convective heat fluxes at all PAS panels during run 3 (N;c;T). The uncertainties reach a maximum after each step-wise change and then decrease towards the steady-state level.

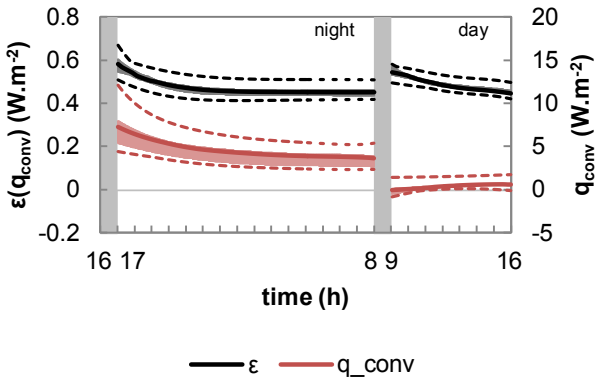

Figure 7 Boxplots (min, 2.5%, median, 97.5%, max) of the uncertainties of the convective heat fluxes at PAS panels during run 3 (N;c;T)

4. Results

4.1 Impact of air supply/exhaust configuration and thermal mass

Figure 8 depicts (a) the temperature and (b) the velocity magnitude courses at the middle floor panel z2 to introduce the experiments. The label 'w,PAS' indicates the inner surface of the PAS panel, 'w,concr' the inner surface of the concrete tiles at vertical v5 and 'a,l' the measuring position at 0.20m above the floor on that same vertical v5. Runs 5 to 8 (without night cooling) exhibit high, almost constant and similar local air and surface temperatures and a moderate, almost constant local air velocity. Most likely, these runs will have a limited cooling capacity during the day regime. Runs 1 to 4 (with night cooling) have different, changing temperatures. At the onset of a new regime, the local air temperature decreases/increases steeply and then gradually follows the exponential decrease/increase of the surface temperature. The local air velocity usually reaches almost instantly its on average constant value. Only during the day regime of run 2 (N;C;t) and run 4 (N;c;t) it first increases for then to decrease. Night cooling (low air temperature, high velocity) effectively cools down the surrounding materials which can absorb heat during the following day regime, at least at the start. Ultimately, every surface temperature would increase above the local air temperature in such cooling cases. However, thermal mass slows down the congruence of the local air temperature and the surface temperature. Because of this, higher temperature differences occur for a longer period of time and, thus, more energy is stored/released. Locating the air supply near the one thermally massive surface (as in run 2 (N;C;t)) leads to the lowest local air temperature and the highest local air velocity and probably the highest convective heat transfer. The jet in run 1 (N;C;T), on the other hand, is broken down for the most part until it hits the concrete tiles (higher local air temperature and lower local air velocity).

Figure 9 confirms that the above predictions are true for the total ventilative cooling performance of the respective runs. It shows the total convective heat flow $Q_{conv,tot}$, i.e. the sum of the convective heat flows at all PAS panels and, when present, concrete tiles, as a function of time. A positive $Q_{conv,tot}$ indicates that the surfaces release heat, a negative one the opposite. First, the impact of the operating conditions catches the eye: the total convective heat flows are usually lower during the day regime than the ones during the night regime. Yet, every total convective heat flow approaches quasi-asymptotically its steady-state level. Next to this, the runs with night cooling show an unmistakably different behaviour: runs 1 to 4 (with night cooling) exhibit a rather low total convective heat flow during the day regime. Run 1 (N;C;T) and run 2 (N;C;t) (with night cooling with thermal mass) even have an overall negative $Q_{conv,tot}$ during the day regime: one or more surfaces absorb heat for the whole period. Moreover, these night cooled runs with thermal mass show a much smaller rate of change of the total convective heat flow than the light equivalent runs do. In addition, these cases are particularly sensitive to the air supply/exhaust configuration. In this case, locating the air supply near the concrete tiles on the floor pays off: $Q_{conv,tot}$ during the day regime is in run 2 (N;C;t) four times as high as the one in run 1 (N;C;T).

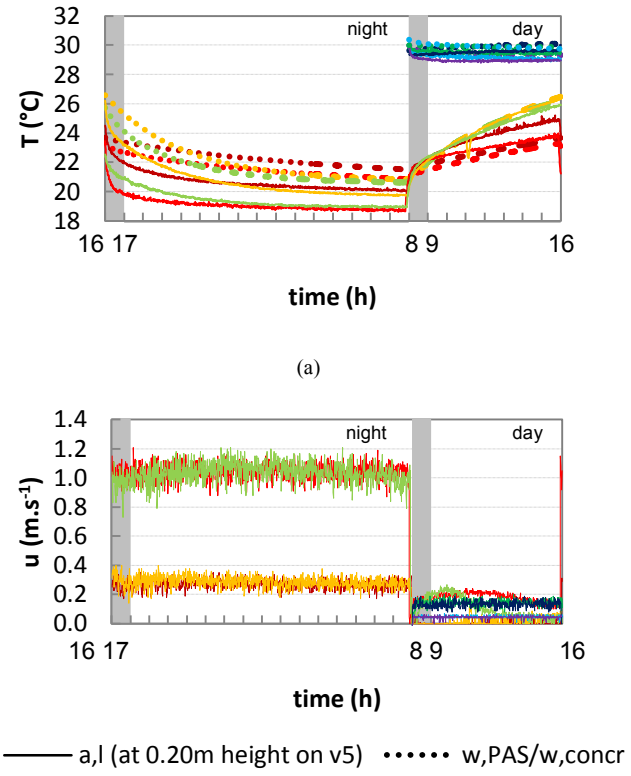

Figure 8 (a) Temperature and (b) velocity at z2 (uncertainty of $T_{w,concr}$, $T_{int,concr}$ and $T_{a,l}$=±0.19°C, uncertainty of $T_{w,PAS}$=±0.07°C, relative uncertainty of $u_{a,l}$=±3% of reading ± 1% of measuring range). For references to colour check the digital version (Table 1)

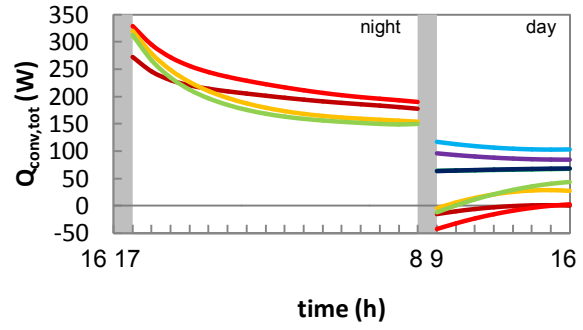

Figure 9 Total convective heat flow at PAS panels (uncertainty of $Q_{conv,tot}$ ranges from ±4.94W to ±7.42W). For references to colour check the digital version (Table 1)

To compare the convection regimes, Figure 10 sets the area-weighted convective heat flux at all PAS panels and, when present, concrete tiles $q_{conv,avg}$ against the difference between the corresponding area-weighted surface temperature $T_{w,avg}$ and the air supply temperature T_{sup}. A positive $q_{conv,avg}$ indicates that the surfaces release heat. This copies the approach used by Artmann et al. (2010) to investigate the convective heat transfer during night cooling. The gradients were interpreted as average heat transfer coefficients $h_{conv,avg}=q_{conv,avg}\cdot(T_{w,avg}-T_{sup})^{-1}$. Such an interpretation also holds for the runs without concrete tiles of underlying study. An average heat transfer coefficient of 0.88W.m^{-2}.K^{-1} applies to the results of the night regime of run 3 (N;c;T) and run 4 (N;c;t). A lower value of about 0.24W.m^{-2}.K^{-1} characterizes the convective heat transfer during the day regime of run 3 (N;c;T), run 4 (N;c;t), run 7 (n;c;T) and run 8 (n;c;t). In these cases the convective heat transfer is insensitive to the air supply/exhaust configuration. However, this does not hold for the cases with concrete tiles on the floor; certainly when also night cooling is applied. Deriving an average heat transfer coefficient is less obvious and the air supply/exhaust configuration does matter. Locating the air supply near the concrete tiles (as in run 2 (N;C;t)) leads to a higher convective heat flux during the night regime by which during the following day regime a lower negative $q_{conv,avg}$ applies.

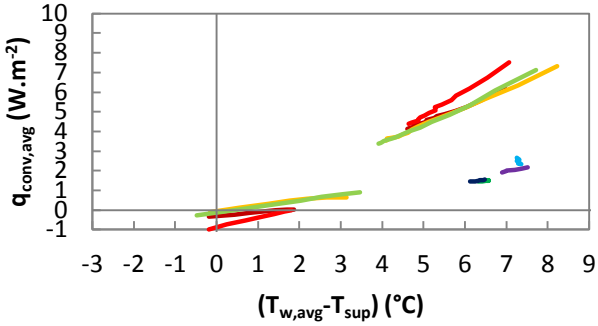

Figure 10 Average convective heat flux vs the difference between the average surface temperature and the air supply temperature. Uncertainty in $(T_{w,avg}-T_{sup})$ is ±0.19°C, uncertainty in $q_{conv,avg}$ ranges from ±0.11W.m^{-2} to ±0.17W.m^{-2} (for references to colour check the digital version (Table 1))

4.2 Comparison to convection correlations

This section sets the convective heat fluxes derived from the temperature measurements against the predictions by existing correlations. To choose an assumedly apt set of correlations, the authors rely on Beausoleil-Morrison's (2000) classification scheme. The five categories included a specific type and cause of the driving force. The convection regimes investigated in the PASLINK cell would be classified under mixed flow. The mechanical forces would be due to an AHU delivering heated/cooled air through ceiling-, floor- or wall-mounted diffusers. The buoyancy forces would be caused by surface-to-air temperature differences. The mixed convection correlations of that same Beausoleil-Morrison would apply. However, in principle they apply merely to cases with one central radial ceiling jet and air change rates higher than 3h^{-1}. Beausoleil-Morrison actually combined the correlations for natural convection of Alamdari and Hammond (1983) and the forced convection equations of Fisher (1995). Eq. (7) shows the ceiling correlation ($T_w<T_{a,avg}$). Here, T_w stands for the surface temperature, $T_{a,avg}$ the indoor air temperature, D_h the hydraulic diameter, T_{sup} the air supply temperature and n the air change rate. The terms in the first brace represent the Alamdari and Hammond correlation. The product in the second brace consists of a scaling factor and the Fisher correlation. This scaling is necessary because Fisher used as a reference the air supply temperature instead of the indoor air temperature.

$$\left\{\left\{\left[1.4\left(\frac{\left|T_w-T_{a,avg}\right|}{D_h}\right)^{\frac{1}{4}}\right]^6+\left[1.63\left|T_w-T_{a,avg}\right|^{\frac{1}{3}}\right]^6\right\}^{3\cdot\frac{1}{6}}+\left\{\left[\frac{T_w-T_{sup}}{\left|T_w-T_{a,avg}\right|}\right]\cdot\left[-0.166+0.484\cdot n^{0.8}\right]\right\}^3\right\}^{\frac{1}{3}} \quad (7)$$

Figure 11 and Figure 82 depict for the night respectively day regime the convective heat flux q_{conv} at (a) the ceiling, (b) the floor and (c) the south wall as a function of the difference between the surface temperature T_w (that is, floor, ceiling…) and the average indoor air temperature $T_{a,avg}$ (i.e. the average of the readings at 0.20m, 1.25m and 2.30m height on all verticals). During the night regime, the predictions by correlations differ the most from the measured convective heat fluxes at the ceiling and in run 2 (N;C;t) and run 4 (N;c;t) from the ones at the floor. At the ceiling, the correlations predict for all runs convective heat fluxes which are three to fourteen times as high as the measured ones. Next, the cases with the air supply at the bottom show a different course: the higher the temperature difference, the lower the measured convective heat flux. At the floor, the correlations underestimate the convective heat flux in run 2 (N;C;t) and run 4 (N;c;t) by 50 to 70%. The results and the predictions of the other two runs correspond reasonably well. At the south wall, the correlations approximate the measured convective heat fluxes in the runs with the air supply at the bottom, i.e. run 2 (N;C;t) and run 4 (N;c;t). Run 1 (N;C;T) and run 3 (N;c;T) exhibit convective heat fluxes which are at most 75% higher than the predictions by correlations. Also note that runs with thermal mass can show an ambiguous relation between the convective heat flux and the temperature difference (e.g. at the floor in run 2 (N;C;t)). During the day regime, again the results at the ceiling and the floor show the largest differences. At the ceiling, the correlations usually overestimate the convective heat flux. Moreover, the correlations do not always produce the expected behaviour: e.g. unreasonably high convective heat fluxes at small temperature differences as in run 3 (N;c;T) and run 4 (N;c;t) or the predictions for runs 5 to 8 are significantly higher than the ones of runs 1 to 4. At the floor, most correlations predict negative convective heat fluxes as the temperature difference is negative. However, the corresponding measured convective heat fluxes are usually positive. Only the results of run 1 (N;C;T) and run 7 (n;c;T) show a rough correspondence. At the south wall, the predictions by correlations for runs 1 to 4 are within the uncertainty bounds of the measured convective heat fluxes. The predicted fluxes for run 5 to 8 are clearly lower than the measured ones.

Most of the above discrepancies are caused by the difference in configuration. As previously mentioned, Beausoleil-Morrison's correlations apply basically to cases with one central radial ceiling jet. This jet would produce a particularly high convective heat flux at the ceiling and lower ones at the other enclosure surfaces. By contrast, in the PASLINK cell, the jet is only able to cover a part of the ceiling during the night regime of cases with the air supply at the top. So it is self-evident that the predicted convective heat fluxes at the ceiling are significantly higher than the measured ones, certainly when the air supply is at the bottom. A similar reasoning explains why predictions at the floor are nowhere close to the measurements in case the air supply is located at the bottom. The influence of a central ceiling jet on the air near the floor is obviously far less than that of a jet at the bottom. The usually positive measured convective heat flux at the floor during the day regime in spite of a negative (T_w-$T_{a,avg}$) is because the (falling) jet locally produces a positive temperature difference. Why the predicted fluxes at the south wall during the night regime of run 1 (N;C;T) and run 3 (N;c;T) are lower than the measured ones is because only then the jet in the PASLINK cell hits the south wall frontally. The several ambiguous relations are explained as follows. The inverse relationship between the measured convective heat flux and the temperature difference during the night regime of run 2 (N;C;t) and run 4 (N;c;t) is because as time goes by the indoor air stratification diminishes and, thus, the difference between the surface temperature and the average indoor air increases. The inhomogeneous temperature distribution also explains the curved relationships of some predictions/measurements. For example, at the beginning of the night regime of run 2 (N;C;t) the measured convective heat flux peaks, but the average indoor air temperature lags. The different predicted heat fluxes for the same temperature differences, on the other hand, occur because Beausoleil-Morrison's correlations include the surface temperature, the average air temperature and the air supply temperature. As a matter of fact, the scaling factor $(T_w-T_{sup}).|T_w-T_{a,avg}|^{-1}$ part of the forced convection component leads to higher convective heat fluxes when the surface temperature differs more from the air supply temperature, as is usually the case in runs 5 to 8. That same scaling factor also causes the unreasonably high convective heat fluxes at small temperature differences (remember the prediction at the ceiling during the day regime of run 3 (N;c;T) and run 4 (N;c;t)). The above comparison of the convective heat fluxes predicted by assumedly apt correlations to the measured ones obtained from dynamic experimental runs clearly indicates the particularity of the available convection correlations.

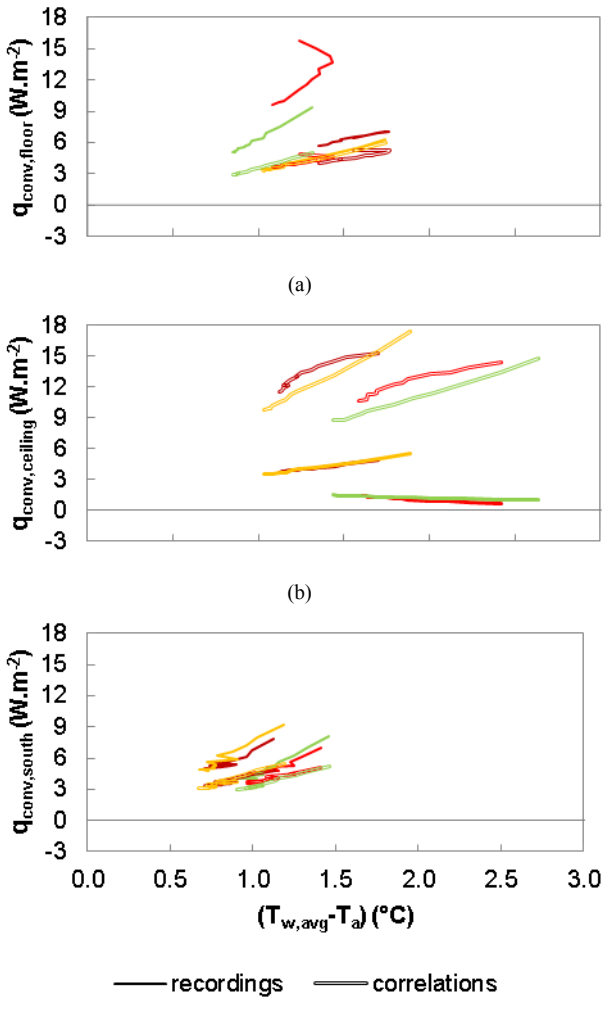

Figure 11 Convective heat flux at (a) the floor, (b) the ceiling and (c) the south wall during night regime as a function of the temperature difference between the respective surface and the average indoor air temperature. For interpretation of the references to colour check the digital version (Table 1)

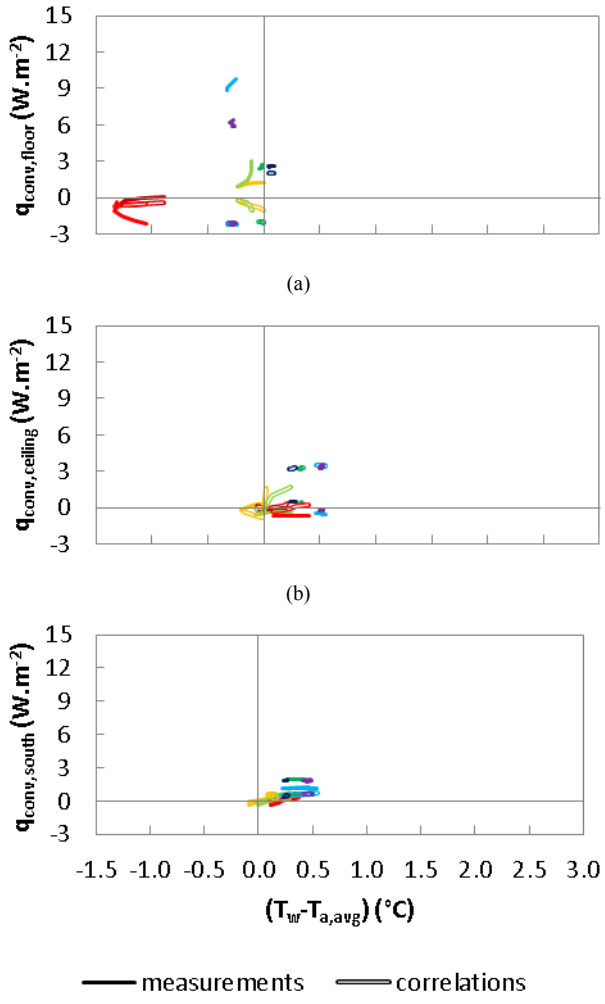

Figure 82 Convective heat flux at (a) the floor, (b) the ceiling and (c) the south wall during day regime as a function of the temperature difference between the respective surface and the average indoor air temperature. For interpretation of the references to colour check the digital version (Table 1)

5. Conclusion: the need of a well-considered design

The above experimental effort is surely no isolated case. However, the suggested approach to derive the convective heat flux and the subsequent uncertainty analysis might be a step forward. The use of a dynamic conduction/radiation model to calculate the convective heat flux introduces without doubt some benefits. For example, it enables a more accurate determination of the convective heat flux and allows to investigate experiments with changing boundary conditions. The actual parametric analysis aimed at identifying the impact of the air supply/exhaust configuration and thermal mass on the convective heat transfer during two typical mixed convection regimes. The results revealed that the air supply/exhaust configuration is important in case high ventilative flow rates are combined with (heterogeneously distributed) thermal mass. For example, locating the air supply near the concrete tiles instead of near the ceiling resulted in an 11% increase of the heat released during night cooling and a 410% increase of heat absorbed during the following day period. The accompanying study on the applicability of existing convection correlations showed that correlations should not be used when the setup and the convection regime differ a lot from those of the corresponding experiments. For example, the assumedly apt correlations of Beausoleil-Morrison predicted at the ceiling convective heat fluxes which were three to fourteen times as high as the measured ones. In other words, it is necessary to further investigate in detail how interrelated room/system parameters affect the mixed convection heat transfer.

Acknowledgements

This work was funded by the Institute for the Promotion of Innovations through Science and Technology in Flanders (IWT-050154). The authors would also like to thank the Belgian Building Research Institute, especially Mr. Voordecker and Mr. L'Heureux.

References

ALAMDARI, F. & HAMMOND, G. P. 1983. Improved data correlations for buoyancy-driven convection in rooms. Building Services Energy Research and Technology, 4, 106-112.

ARTMANN, N., JENSEN, R. L., MANZ, H. & HEISELBERG, P. 2010. Experimental investigation of heat transfer during night-time ventilation. Energy and Buildings, 366-74.

BEAUSOLEIL-MORRISON, I. 2000. The adaptive coupling of heat and air flow modelling within dynamic whole-building simulation. PhD, University of Strathclyde.

CEN 2008. EN 13163: Thermal insulation products for buildings - Factory made products of expanded polystyrene (EPS) - Specification. Brussels.

DIN 1993. DIN 4715: Raumkühlflächen - Leistungsmessung bei freier Strömung Prüfregeln. Berlin.

DOMINGUEZ-MUNOZ, F., ANDERSON, B., CEJUDO-LOPEZ, J. M. & CARRILLO-ANDRES, A. 2010. Uncertainty in the thermal conductivity of insulation materials. Energy and Buildings, 42, 2159-2168.

FISHER, D. E. 1995. An experimental investigation of mixed convection heat transfer in a rectangular enclosure. PhD, University of Illinois.

GOETHALS, K., BREESCH, H. & JANSSENS, A. 2011. Sensitivity analysis of predicted night cooling performance to internal convective heat transfer modelling. Energy and Buildings, 43, 2429-2441.

ISO 2007. ISO 12465: Plywood - Specifications. Geneva.

LOMAS, K. J., MARTIN, C., EPPEL, H., WATSON, M. & BLOOMFIELD, D. 1994. Empirical validation of thermal building simulation programs using test room data - Volume 1: Final report. International Energy Agency.

NBN 2009. NBN EN ISO 6946: Building components and building elements - Thermal resistance and thermal transmittance - Calculation method. Brussels.

WANG, A. B. & TRAVNICEK, Z. 2001. On the linear heat transfer correlation of a heated circular cylinder in laminar crossflow using a new representative temperature concept. International Journal of Heat and Mass Transfer, 44, 4635-4647.